

Ambiguities in fits of binary lens galactic microlensing events

M. Dominik

Institut für Physik, Universität Dortmund, D-44221 Dortmund, Germany

Abstract

For observed galactic microlensing events only one fit is usually presented, though, especially for a binary lens, several fits may be possible. This has been shown for the MACHO LMC#1 event (Dominik & Hirshfeld 1996). Here I discuss the strong binary lens events OGLE#7 and DUO#2. It is shown that several models with a large variety of parameters are possible. For most of the fits, $1\text{-}\sigma$ -bounds on the fit parameters are given. The variation of the parameters within these bounds is in some cases considerable.

1 Introduction

Some of the observed galactic microlensing events show a signature of a binary lens. The first such event discovered was MACHO LMC#1, where its binary nature has been discussed by Dominik & Hirshfeld (1994, 1996). An explanation with a binary lens has also been proposed for OGLE#6 by Mao & Di Stefano (1995). Neither of these events involves crossings of the source trajectory with the caustics, which would result in sharp spikes in the light curves, and are called weak binary lens events for this reason. In contrast, the events OGLE#7 (Udalski et al. 1994), DUO#2 (Alard et al. 1995), and MACHO LMC#9 (Bennett et al. 1996) involve such caustic crossings, and are therefore called strong binary lens events. The MACHO collaboration claims 3 additional binary lens events in their data obtained with the alert system, namely 95-BLG-12, 96-BLG-3 and 96-BLG-9, where the last event may be due to a weak binary lens, whereas the others are strong binary lens events (Stubbs et al. 1997).

Except for the discussion of the MACHO LMC#1 event (Dominik & Hirshfeld 1996), only one fit has been presented for each of the other binary lens events. However, as shown for MACHO LMC#1, there may be several solutions. For the events OGLE#7 and DUO#2 this is shown explicitly in this paper. Section 2 reviews the basics of galactic microlensing with binary lenses, Section 3 gives the discussion of the OGLE#7 event, while the DUO#2 event is discussed in Section 4. In Section 5 the results are summarized.

2 Galactic microlensing with binary lenses

Consider a lens at a distance D_d from the observer, a source at a distance D_s from the observer, and let D_{ds} be the lens-source distance. The Einstein radius for a lens of mass M is then given by

$$r_E = \sqrt{\frac{4GM}{c^2} \frac{D_d D_{ds}}{D_s}}. \quad (1)$$

Further consider an optical axis through observer and lens center and planes perpendicular to it at the position of the lens (lens plane) and the source (source plane) centered at the optical axis. Let the source be located at $\vec{\eta} = \frac{D_s}{D_d} r_E \vec{y}$ in the source plane and let a light ray pass from the source to the observer through the lens plane at $\vec{\xi} = r_E \vec{x}$.

For a binary lens consisting of a mass with fraction m_1 of the total mass M at $(r_{hd}, 0)$ and a mass with fraction $m_2 = 1 - m_1$ at $(-r_{hd}, 0)$, where $r_{hd} = \chi r_E$, the coordinates \vec{x} and \vec{y} are related by the lens equation

$$y_1(x_1, x_2) = x_1 - m_1 \frac{x_1 - \chi}{(x_1 - \chi)^2 + x_2^2} - (1 - m_1) \frac{x_1 + \chi}{(x_1 + \chi)^2 + x_2^2}, \quad (2)$$

$$y_2(x_1, x_2) = x_2 - m_1 \frac{x_2}{(x_1 - \chi)^2 + x_2^2} - (1 - m_1) \frac{x_2}{(x_1 + \chi)^2 + x_2^2}, \quad (3)$$

which gives the true source position as a function of the observed image position. For a given source position, there are either 3 or 5 images. To obtain the images for a given source position \vec{y} one has to solve the lens equation numerically.

The magnification μ of an image at \vec{x} is given by the inverse of the Jacobian determinant of the mapping, i.e.

$$\mu(\vec{x}) = \frac{1}{\left| \det \left(\frac{\partial \vec{y}}{\partial \vec{x}} \right) \right|}, \quad (4)$$

and the total magnification of a (point) source $\tilde{\mu}(\vec{y})$ is given as the sum of the magnifications of the individual images. A (point) source is located on a caustic if $\mu(\vec{x})$ diverges for at least one image \vec{x} . The magnification of an extended source is obtained by integrating over the point source magnifications.

Let the source move on a straight line with a velocity v_{\perp} projected onto the lens plane transverse to the line-of-sight observer-lens, so that it moves one Einstein radius in the lens plane in the time $t_E = \frac{r_E}{v_{\perp}}$.¹ For the fits, a timescale $t_c = 2t_E$ is used. In addition, the following parameters are used (see Figure 2)²: The source trajectory projected to the lens plane has the closest approach to the origin at the time t_{\max} and the distance $r_{\min} = u_{\min} r_E$. The angle α is measured between the x_1 -direction and the direction of motion of the source. To get uniqueness in parameter space, the sign of the velocity of the source is chosen so that the midpoint of the lens system is on the right hand side of the line traced in time by the source and the parameter ranges are $u_{\min} \geq 0$, $0 \leq \alpha < \pi$ and $0 \leq m_1 \leq 1$.

The observed amplification of the source object as a function of time $A(t)$ has been calculated efficiently by solving the lens equation for the whole source trajectory simultaneously (Dominik 1995) and by determining the magnification from the images with Eq. (4).

Another parametrization for binary lenses has been used by Mao & Di Stefano (1995). The main difference is that they refer the closest approach of the source to the center of mass of the lens system and not to the midpoint. The translation between the parameter sets is shown in Table 1.

Mao & Di Stefano \rightarrow Dominik	Dominik \rightarrow Mao & Di Stefano
$\alpha[\text{rad}] = \frac{\pi}{180} \vartheta[^\circ]$	$\vartheta[^\circ] = \frac{180}{\pi} \alpha[\text{rad}]$
$m_1 = \frac{q}{q+1}$	$q = \frac{m_1}{1-m_1}$
$\chi = a/2$	$a = 2\chi$
$t_c = 2t_E$	$t_E = t_c/2$
$r_{\min} = b - \frac{a}{2} \frac{q-1}{q+1} \sin \vartheta$	$b = r_{\min} - \chi(1-2m_1) \sin \alpha$
$t_{\max} = t_b - \frac{a}{2} \frac{q-1}{q+1} t_E \cos \vartheta$	$t_b = t_{\max} - \chi(1-2m_1) \frac{t_c}{2} \cos \alpha$

Table 1: The translation between different parameter sets for binary lens models

The amount of additional light contributed by other objects than the 'source' is described by the blending parameter f . It gives the contribution of the light of the unlensed source to the total light. If $A(t)$ denotes the amplification of the source, the observed amplification is given by

$$A_{\text{tot}} = fA(t) + 1 - f. \quad (5)$$

3 OGLE #7

The OGLE#7 event (Udalski et al. 1994, hereafter USM) is the first event observed which shows the signature of a strong binary lens. In contrast to the MACHO LMC#1 event, it is clear that a single lens

¹Note that this is equivalent to letting the lens move with v_{\perp} into the opposite direction. Further note that if the fixed source is on the right side of the lens trajectory, a corresponding fixed lens is on the right side of the source trajectory.

²These parameters coincide with those which have been used in (Dominik & Hirshfeld 1994, 1996)

cannot explain the data, because it will produce neither spikes nor a plateau formed like a U, irrespective of whether the source is a binary or not or whether the objects are extended. A first fit to the data has been presented in USM. However, several binary lens fits are possible. In Tables 2 and 3, I present the results of 8 different fits. The χ^2 corresponds to the original errors given by the OGLE collaboration. The errors on the parameters correspond to projections of the hypersurface $\Delta\chi^2 = \chi^2 - \chi_{\min}^2 = 1$ onto the axes in parameter space. The characteristic time ranges from 162 d (BL0) to 1470 d (BL6) which means that the expected total mass ($\propto t_c^2$) varies by a factor of 80. The mass ratio ranges from about 1 (BL0, BL6, BL7) to 16 (BL). The contribution of external light (blending) at the minimum light ranges from 17 % (BL9) to 94 % (BL). Note that some of the errors on t_c are large: For BL2 the 1- σ error is about 25 % of the value, for BL7, BL1, BL3, and BL9 the 1- σ errors are also about 10–20 % of the value of t_c . The second pair of caustic crossings for the BL-fit and the caustic crossings on the triangle shaped caustic for the BL6-fit posed additional problems for the calculation of the error bounds, so that no error bounds are shown for these fits.

parameter	BL2	BL0	BL1	BL7
t_c [d]	345_{-82}^{+95}	$161.8_{-6.9}^{+6.8}$	291_{-19}^{+41}	350_{-39}^{+52}
t_{\max} [d]	$1147.6_{-7.4}^{+4.7}$	$1173.3_{-2.0}^{+2.5}$	$1164.6_{-1.5}^{+1.2}$	$1150.86_{-10.5}^{+0.47}$
χ	$0.400_{-0.028}^{+0.041}$	$0.565_{-0.010}^{+0.011}$	$0.387_{-0.013}^{+0.030}$	$0.496_{-0.011}^{+0.021}$
m_1	$0.268_{-0.054}^{+0.082}$	$0.506_{-0.014}^{+0.029}$	$0.397_{-0.015}^{+0.089}$	$0.518_{-0.043}^{+0.022}$
α [rad]	$2.517_{-0.062}^{+0.028}$	$2.297_{-0.048}^{+0.044}$	$1.635_{-0.026}^{+0.025}$	$0.135_{-0.099}^{+0.025}$
u_{\min}	$0.013_{-0.012}^{+0.006}$	$0.048_{-0.006}^{+0.013}$	$0.01100_{-0.020}^{+0.00088}$	$0.539_{-0.060}^{+0.054}$
m_{base}	$-17.5299_{-0.0077}^{+0.0079}$	$-17.5171_{-0.0070}^{+0.0071}$	$-17.5260_{-0.0088}^{+0.0077}$	$-17.5487_{-0.013}^{+0.0091}$
f	$0.241_{-0.041}^{+0.066}$	$0.557_{-0.022}^{+0.020}$	$0.243_{-0.014}^{+0.017}$	$0.618_{-0.019}^{+0.019}$
χ_{\min}^2	133.94	137.73	137.93	140.25

Table 2: OGLE #7: Fits for a strong binary lens event

The fit of USM corresponds to the BL0-fit. Table 4 shows the parameters of the BL0-fit in the parametrization used in USM and the parameters quoted there. Note that their m_0 is the magnitude of the lensed component, while m_{base} corresponds to the minimum light observed, i.e. the light from the lensed and the unlensed component. These quantities are therefore related by

$$m_0 = -m_{\text{base}} - 2.5 \lg f. \quad (6)$$

If one accepts the given error bars of the data points, one sees that the values of χ_{\min}^2 are very bad (see Table 5). If one adapts the size of the error bars to the tail data points in the same way as for the MACHO LMC#1 event (Dominik & Hirshfeld 1996), but with Gaussian errors³, defining all data points for $t < 900$ d as belonging to the 'tail', one obtains a scaling factor of $\gamma = 1.597$, which means that the errors are enlarged by about 60 %. The probabilities for the fits become ≥ 84 % for all fits and ≥ 95 % for all fits except for BL3 and BL9. If one looks carefully at the light curve and the data, one sees that

³As shown for the MACHO LMC#1 event (Dominik 1996) the results do not differ much if one uses a larger rescaling factor with a distribution with smaller tail or a smaller rescaling factor with a distribution with larger tail. Since there are only a few data points in the tail region (32), the extraction of non-Gaussian behaviour is not successful (Dominik 1996).

parameter	BL6	BL	BL3	BL9
t_c [d]	1470.84	1299.68	440.56^{+43}_{-26}	495^{+73}_{-70}
t_{\max} [d]	2149.92	1380.10	$1168.4^{+2.1}_{-2.7}$	$1160.93^{+0.95}_{-2.4}$
χ	0.2813	0.3725	$0.854^{+0.044}_{-0.039}$	$0.736^{+0.014}_{-0.010}$
m_1	0.510	0.059	$0.759^{+0.081}_{-0.11}$	$0.938^{+0.024}_{-0.009}$
α [rad]	2.050	0.414	$1.567^{+0.031}_{-0.025}$	$1.942^{+0.043}_{-0.054}$
u_{\min}	0.649	0.068	$0.316^{+0.077}_{-0.064}$	$0.086^{+0.027}_{-0.023}$
m_{base}	-17.5868	-17.5555	$-17.5538^{+0.0079}_{-0.0096}$	$-17.639^{+0.031}_{-0.030}$
f	0.667	0.057	$0.578^{+0.052}_{-0.064}$	$0.829^{+0.032}_{-0.043}$
χ_{\min}^2	141.49	143.41	150.95	160.06

Table 3: OGLE #7: Fits for a strong binary lens event

parameter	BL0	Udalski et al.
t_E [d]	80.88	80
t_b [d]	1172.89	1172.5
a	1.1309	1.14
q	1.024	1.02
θ [°]	131.68	138.3
b	0.0532	0.050
m_0	18.152	18.1
f	0.5573	0.56

Table 4: OGLE #7: The BL0-fit and the fit of USM

the data point in the tail at $t = 806.60603$ and $I = 17.794$ contributes about 33 to the total χ^2 . If one omits this discrepant point, one gets a rescaling factor of $\gamma = 1.247$ and the results shown in Table 6. If one assumes that the discrepant point in the tail is due to a measurement error, and taking into account that the error bars may be about 15-25 % too small, one can accept all 8 models (see Table 6). If one does not ascribe the discrepant point to a measurement error, one has to accept the large rescaling factor to allow the tail to be constant. Also in this case, all the fits are acceptable. Note that the errors may show some non-Gaussian behaviour. This behaviour is effectively absorbed into the rescaling factor in my analysis.

	BL2	BL0	BL1	BL7	BL6	BL	BL3	BL9
χ_{\min}^2	133.94	137.73	137.93	140.25	141.49	143.41	150.95	160.06
$\sqrt{2\chi_{\min}^2} - \sqrt{2n-1}$	4.160	4.390	4.402	4.542	4.615	4.729	5.169	5.685
$P(\chi^2 \geq \chi_{\min}^2)$	$2 \cdot 10^{-5}$	$6 \cdot 10^{-6}$	$5 \cdot 10^{-6}$	$3 \cdot 10^{-6}$	$2 \cdot 10^{-6}$	$1 \cdot 10^{-6}$	$1 \cdot 10^{-7}$	$7 \cdot 10^{-9}$

Table 5: OGLE #7: χ_{\min}^2 and the corresponding probability without rescaling

	BL2	BL0	BL1	BL7	BL6	BL	BL3	BL9
χ_{\min}^2	64.98	66.92	67.55	68.65	69.71	70.37	76.60	80.86
$\sqrt{2\chi_{\min}^2} - \sqrt{2n-1}$	-0.807	-0.638	-0.583	-0.489	-0.399	-0.343	0.171	0.510
$P(\chi^2 \geq \chi_{\min}^2)$	79 %	74 %	72 %	69 %	66 %	63 %	43 %	30 %

Table 6: OGLE #7: χ_{\min}^2 and the corresponding probability without discrepant point with rescaling

The light curves for the fits are shown in Figure 3 and the structure of the caustics together with the source trajectory can be seen in Figure 3. The distance scale used is projected Einstein radii ($r'_E = \frac{D_s}{D_d} r_E$) of the total mass in the source plane. The intersections of the source trajectory with the caustics and the projected positions of the lens objects are indicated by small crosses. The tip of the arrow on the trajectory denotes the closest approach to the coordinate origin.

4 DUO #2

The DUO#2 event has been reported by Alard, Mao, and Guibert (1995), hereafter AMG, where a fit with a strong binary lens is presented. The corresponding fit parameters using my parameter set are shown in Table 7. For 116 data points, a χ^2 of 89 is reached, where the source is treated as extended ($R_{\text{src}} \lesssim 10^{-2}$) and limb-darkened with $\tilde{u}_{\text{blue}} = 0.6$ and $\tilde{u}_{\text{red}} = 0.5$, where the brightness profile of the source is of the form

$$f(r, \tilde{u}) = \tilde{u} \sqrt{1 - r^2} + 1 - \tilde{u}, \quad (7)$$

r being the ratio of the actual radius and the total radius.

Here I show additional possible fits using a static binary lens and a point source. I have omitted one occurrence of a data point which appeared twice in the data I have received from C. Alard, so that I use 115 data points and not 116 data points as in AMG. Moreover, I use the magnitude values for the fit and not the amplification values as used for the fit in AMG (S. Mao, private communication). From this, only a small difference results (Dominik 1996), the χ^2_{\min} differs only by about 2 units and the fit parameters show only small differences which are well within the bounds corresponding to $\Delta\chi^2 = 1$. The analysis of the tail data points ($t < 70$ d or $t > 100$ d) yielded most-likely scaling factors $\gamma_{\text{blue}} = 0.912$ for 63 data points and $\gamma_{\text{red}} = 0.828$ for 25 data points. These values are close to 1 (note that there are only a few tail data points), so that the tail seems to be consistent with a constant brightness and no further scaling is used in this discussion. The results of the fits are shown in Tables 8 and 9. The quoted error bounds correspond to projections of the hypersurface $\Delta\chi^2 = 1$ onto the axes in parameter space. An asterisk (*) denotes that the numerical routines have ended up at a jump discontinuity. It is not yet clear if this is a real effect or if it is due to difficulties in the computation. There appear additional minima, whose $\Delta\chi^2 \leq 1$ -regions include other minima with smaller χ^2 . In particular, this is a problem for the BL1-, BL2-, and the BL4-fit which also makes the calculation of the error bounds difficult, so that they are not shown in the tables for these fits. This behavior is influenced by the fact that there are only a few data points to constrain the shape of the light curve in the peak region.

parameter	DUO#2 in AMG
t_c [d]	17
t_{\max} [d]	85.19
χ	0.605
m_1	0.752
α [rad]	1.490
u_{\min}	0.096
$m_{\text{base,blue}}$	-20.21
$m_{\text{base,red}}$	-18.55
f_{blue}	0.73
f_{red}	0.70

Table 7: DUO #2: Fit of AMG

Taking into account the error bounds, the BL-fit seems to coincide with the fit in AMG, except for the small lower bound on χ , which however may be relict of computational problems. Near the parameters for the BL-fit, I have started a fit including an extended source. As for the fit of AMG, the source brightness profile has been fixed to a limb-darkening profile with $\tilde{u}_{\text{blue}} = 0.6$ and $\tilde{u}_{\text{red}} = 0.5$. The resulting fit parameters are shown in Table 10. Note that this fit gives only a slightly better χ^2_{\min} than the BL-fit with a point source. The parameters coincide with the BL-fit as well as with the fit of AMG. It is not clear to me how the $\chi^2_{\min} = 89$ of AMG is reached. For their fit parameters (S. Mao, private communication), I obtain a χ^2 which is larger than the χ^2_{\min} for the extended source fit. One sees that the BL- and the BL4-fit give good explanations of the observed data, while the BL2-, BL3-,

parameter	BL	BL4	BL2
t_c [d]	$18.9^{+2.5}_{-1.5}$	23.79	16.40
t_{\max} [d]	$85.234^{+0.075}_{-0.062}$	89.247	88.351
χ	$0.6434^{+0.050}_{-0.0011*}$	0.4058	0.4571
m_1	$0.759^{+0.005}_{-0.026}$	0.176	0.829
α [rad]	$1.496^{+0.023}_{-0.024}$	0.670	2.576
u_{\min}	$0.157^{+0.025*}_{-0.043*}$	0.00684	0.0406
$m_{\text{base,blue}}$	$-20.2077^{+0.0061}_{-0.0059}$	-20.2087	-20.2046
$m_{\text{base,red}}$	$-18.575^{+0.011}_{-0.011}$	-18.5777	-18.5733
f_{blue}	$0.708^{+0.035}_{-0.048}$	0.260	0.418
f_{red}	$0.702^{+0.044}_{-0.054}$	0.266	0.441
χ^2_{\min}	109.45	111.57	131.17
$n = \#$ d.o.f.	105	105	105
$\sqrt{2\chi^2_{\min}} - \sqrt{2n-1}$	0.338	0.481	1.740
$P(\chi^2 \geq \chi^2_{\min})$	37 %	32 %	4 %

Table 8: DUO #2: Fits for a strong binary lens event

parameter	BL3	BL5	BL1
t_c [d]	$14.95^{+0.94}_{-0.93}$	$12.30^{+0.21*}_{-0.57}$	14.40
t_{\max} [d]	$85.69^{+0.15}_{-0.24}$	$84.29^{+0.06*}_{-0.28}$	85.99
χ	$0.7832^{+0.0068}_{-0.0078}$	$0.495^{+0.009}_{-0.005*}$	0.649
m_1	$0.263^{+0.036}_{-0.024}$	$0.195^{+0.030}_{-0.031}$	0.394
α [rad]	$0.536^{+0.022}_{-0.030}$	$2.260^{+0.071}_{-0.044*}$	0.423
u_{\min}	$0.053^{+0.011}_{-0.017}$	$0.161^{+0.017}_{-0.016}$	0.261
$m_{\text{base,blue}}$	$-20.2075^{+0.0065}_{-0.0062}$	$-20.1980^{+0.0057}_{-0.0057}$	-20.2059
$m_{\text{base,red}}$	$-18.574^{+0.011}_{-0.011}$	$-18.564^{+0.011}_{-0.011}$	-18.573
f_{blue}	$0.886^{+0.024}_{-0.037*}$	$0.548^{+0.042}_{-0.042}$	0.803
f_{red}	$0.872^{+0.037}_{-0.042}$	$0.529^{+0.044}_{-0.044}$	0.795
χ^2_{\min}	134.96	137.63	168.39
$n = \#$ d.o.f.	105	105	105
$\sqrt{2\chi^2_{\min}} - \sqrt{2n-1}$	1.973	2.134	3.89
$P(\chi^2 \geq \chi^2_{\min})$	2 %	2 %	$5 \cdot 10^{-5}$

Table 9: DUO #2: Fits for a strong binary lens event

parameter	binary lens, extended source
t_c [d]	19.1
t_{\max} [d]	85.18
χ	0.626
m_1	0.738
α [rad]	1.447
u_{\min}	0.159
$m_{\text{base,blue}}$	-20.207
$m_{\text{base,red}}$	-18.575
f_{blue}	0.665
f_{red}	0.657
R_{src}	0.0012
χ_{\min}^2	107.28
$n = \#$ d.o.f.	104
$\sqrt{2\chi_{\min}^2 - \sqrt{2n - 1}}$	0.260
$P(\chi^2 \geq \chi_{\min}^2)$	40 %

Table 10: DUO #2: Fit for a strong binary lens and an extended source

and the BL5-fit give worse results, although they are not totally excluded. The BL1-fit gives such a low probability that it is excluded. Light curves of the peak region ($70 \text{ d} \leq t \leq 100 \text{ d}$) for both spectral bands together with the data points are shown in Figures 4 and 4, where the upper curve refers to the blue band and the lower curve refers to the red band. Note that the largest differences between the BL-fit and the extended source fit near the BL-parameters occur in the peak after the caustic crossings, not in the caustic crossings themselves.

The configurations for the different models are shown in Figure 4, where the caustics are shown together with the trajectory of the moving point source. The projected positions of the lens objects and the intersections of the source trajectory with the caustics are indicated by small crosses. All distances are measured in Einstein radii r_E if the projection to the lens plane is considered or in projected Einstein radii r'_E if the projection to the source plane is considered.

A peak near a caustic crossing can also be modeled in a different way with a rotating binary lens. With parameters similar to those used for the model BL0 for OGLE#7, a peak after the caustic crossing can be modeled by including the rotation (Dominik 1997b).

5 Summary of results

It has been shown that there are several models which describe the observed strong binary lens events OGLE#7 and DUO#2. A large variety of timescales results, so that the expectation value for the mass (see Dominik 1997a) differs by a factor of 80 for the different fits for OGLE#7. In addition, the uncertainty in t_c for a given fit as given by the $1 - \sigma$ -bound is as large as 25 % for OGLE#7, which is substantially larger than for MACHO LMC#1 or events described by single point-mass lenses. Some part of the non-uniqueness of the fits is due to the sampling rate (especially for DUO#2). However, it has been shown for MACHO LMC#1 (Dominik & Hirshfeld 1996), that even for a good sampling, the fits BA and BL, which are completely different, cannot be discriminated. This shows that it is of importance to look for all possible fits. To claim the existence of a planet from a microlensing light curve, one has to study all possible models and to consider the uncertainties of the fit parameters (as given e.g. by $1 - \sigma$ -bounds). From these fit parameters, information about the physical quantities (mass, separation) can be obtained (Dominik 1997a).

Acknowledgements

I would like to thank S. Mao for some discussions on the subject, C. Alard for sending me the data of the DUO#2 event, the OGLE collaboration for making available their data, and A. C. Hirshfeld for reading the manuscript.

References

- [1] Alard C., Mao S., Guibert J., 1995, A&A 300, L17

- [2] Bennett D. P., Alcock C., Allsman R. A., et al., 1996, A binary lensing event toward the LMC: Observations and dark matter implications, Proceedings of the Dark Matter '96 conference, Santa Monica CA, USA
- [3] Dominik M., 1995, *A&AS* 109, 597
- [4] Dominik M., 1996, PhD thesis, Universität Dortmund
- [5] Dominik M., 1997a, Estimating physical quantities for an observed galactic microlensing event, preprint astro-ph/9701035
- [6] Dominik M., 1997b, Galactic microlensing with rotating binaries, preprint astro-ph/9702039
- [7] Dominik M., Hirshfeld A.C., 1994, *A&A* 289, L31
- [8] Dominik M., Hirshfeld A.C., 1996, *A&A* 313, 841
- [9] Mao S., Di Stefano R., 1995, *ApJ* 440, 22
- [10] Stubbs C., et al. (MACHO collaboration), 1997, <http://darkstar.astro.washington.edu>
- [11] Udalski A., Szymański M., Mao S., et al., 1994, *ApJ* 436, L103

FIGURE CAPTIONS

- Figure 1:** The geometry of a binary lens event
- Figure 2:** OGLE#7: Light curves for the different binary lens fits and measured data points in I-band. From left to right, top to bottom: (a) BL2, (b) BL0, (c) BL1, (d) BL7, (e) BL6, (f) BL, (g) BL3, (h) BL9.
- Figure 3:** OGLE#7: Caustics and source trajectory for the different binary lens fits. The distance is measured in projected Einstein radii of the total mass. Small crosses indicate crossings of the source trajectory with the caustics and the projected positions of the point masses. From left to right, top to bottom: (a) BL2, (b) BL0, (c) BL1, (d) BL7, (e) BL6, (f) BL, (g) BL3, (h) BL9.
- Figure 4:** DUO #2: Light curves for the different binary lens fits and measured data points. Light curve for the blue spectral band on the top and light curve for the red spectral band on the bottom. From left to right, top to bottom: (a) BL, (b) BL4, (c) BL2, (d) BL3.
- Figure 5:** DUO #2: Light curves for the different binary lens fits and measured data points. Light curve for the blue spectral band on the top and light curve for the red spectral band on the bottom. From left to right: (a) BL5, (b) BL1.
- Figure 6:** DUO #2: Light curves for the fit near BL with an extended source and the measured data points. Light curve for the blue spectral band on the top and light curve for the red spectral band on the bottom.
- Figure 7:** DUO #2: Caustics and source trajectory for the different binary lens fits. From left to right, top to bottom: (a) BL, (b) BL4, (c) BL2, (d) BL3, (e) BL5, (f) BL1.

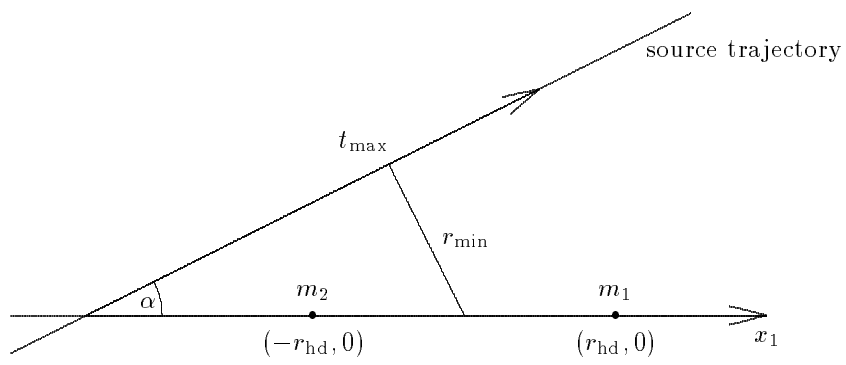


Figure 1

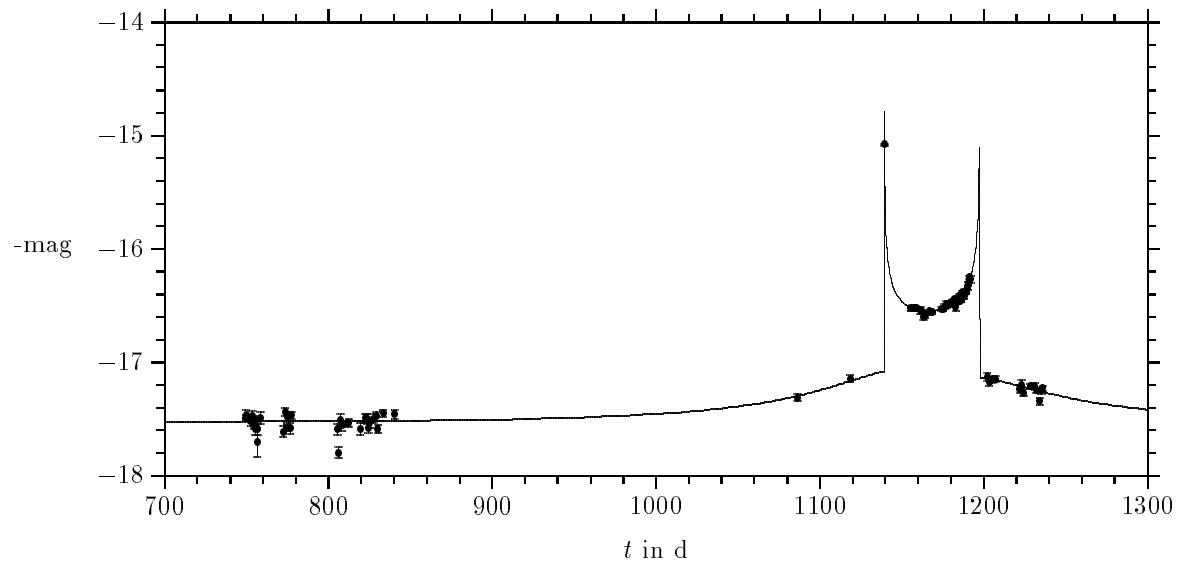


Figure 2a

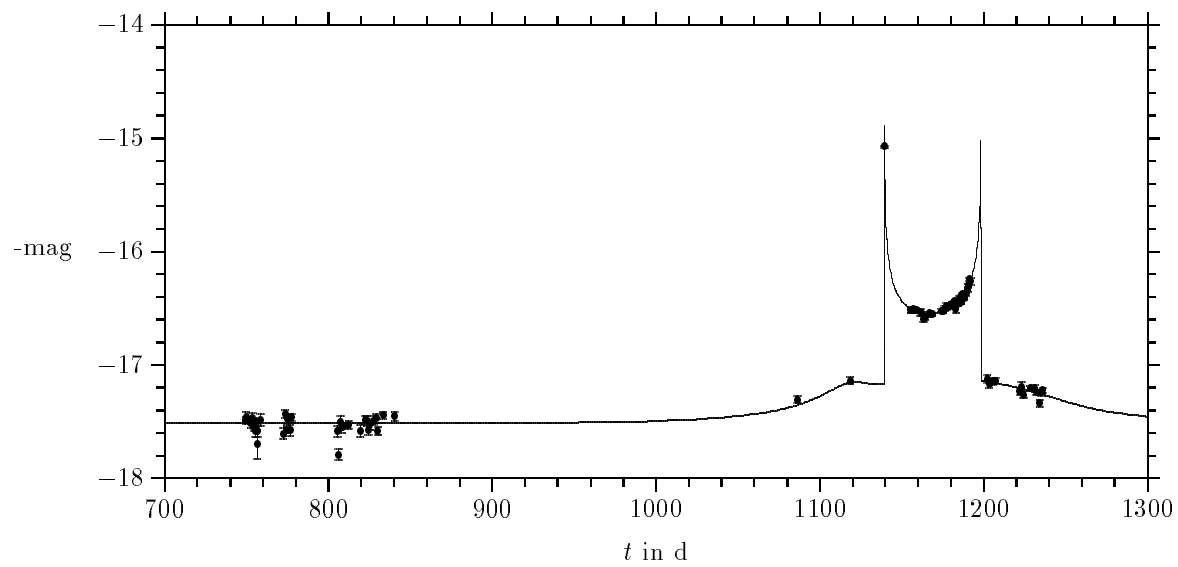


Figure 2b

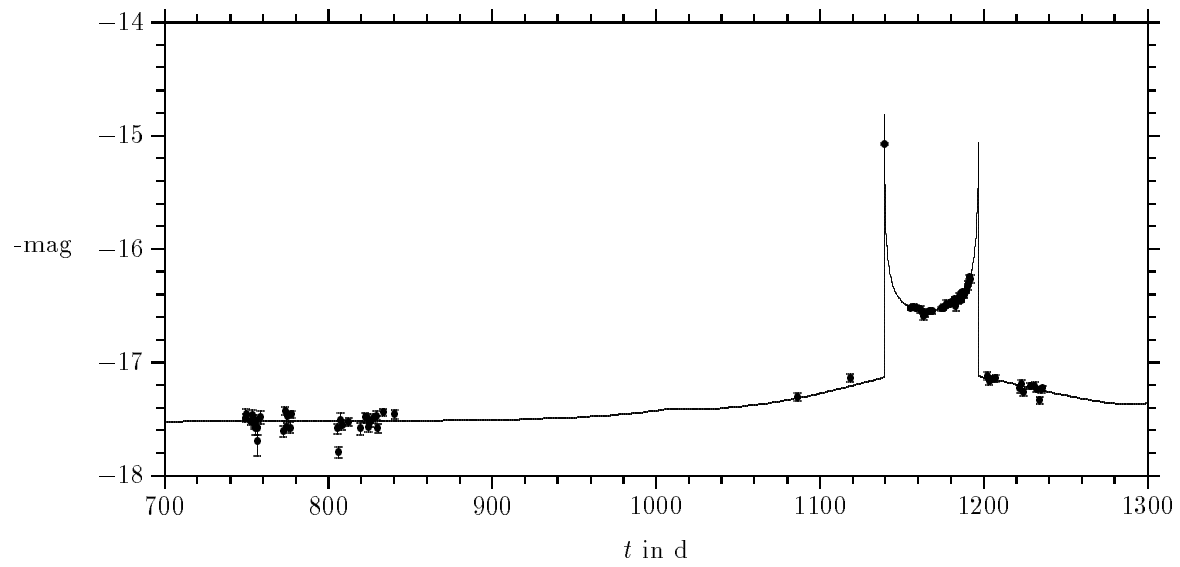


Figure 2c

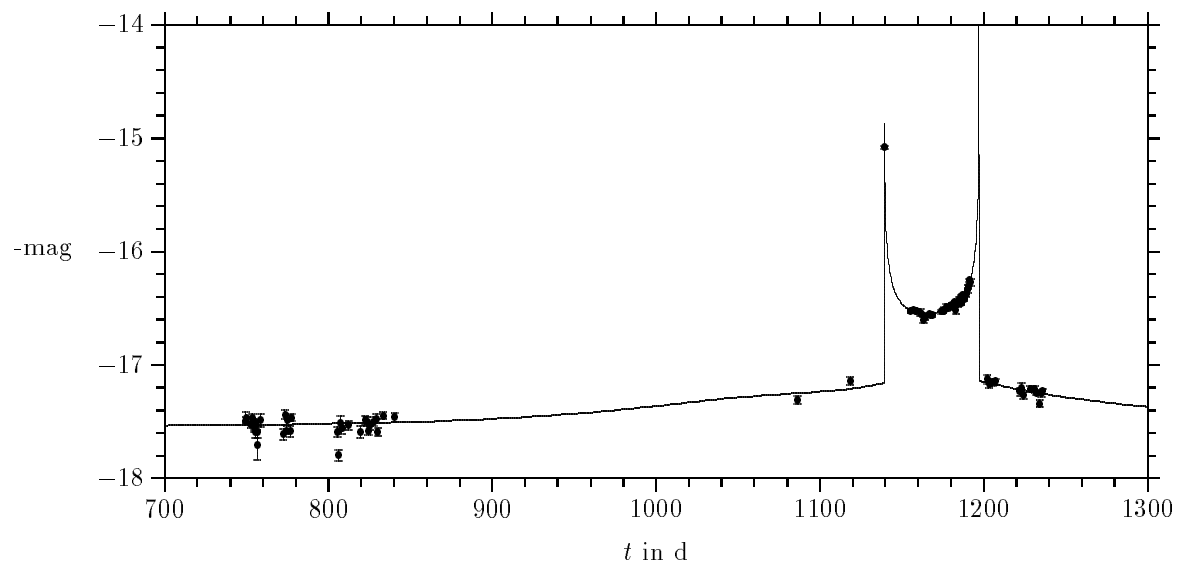


Figure 2d

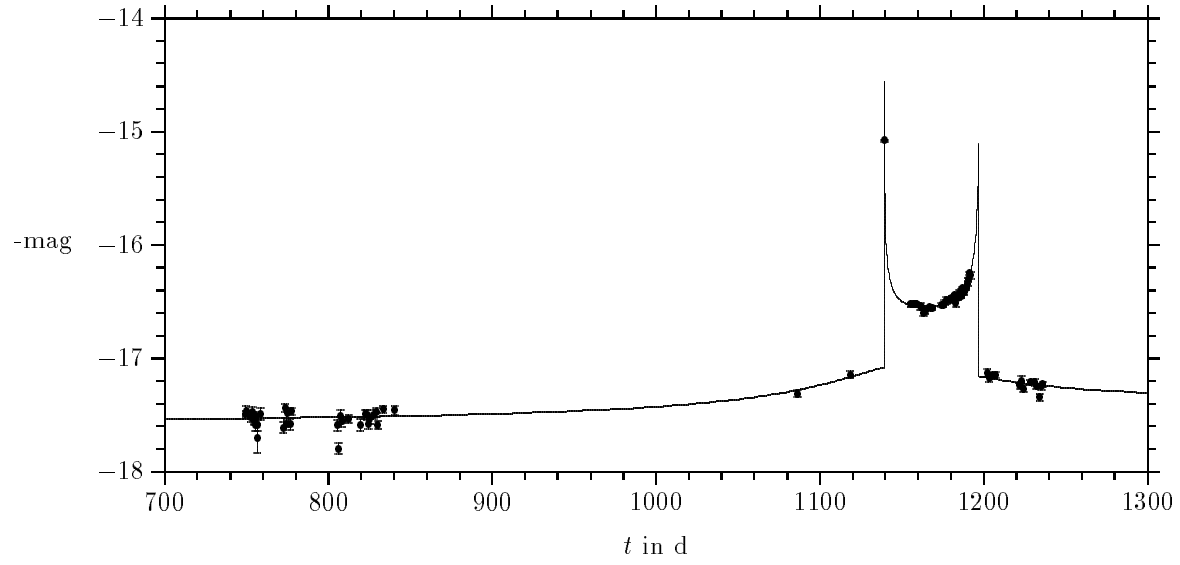


Figure 2e

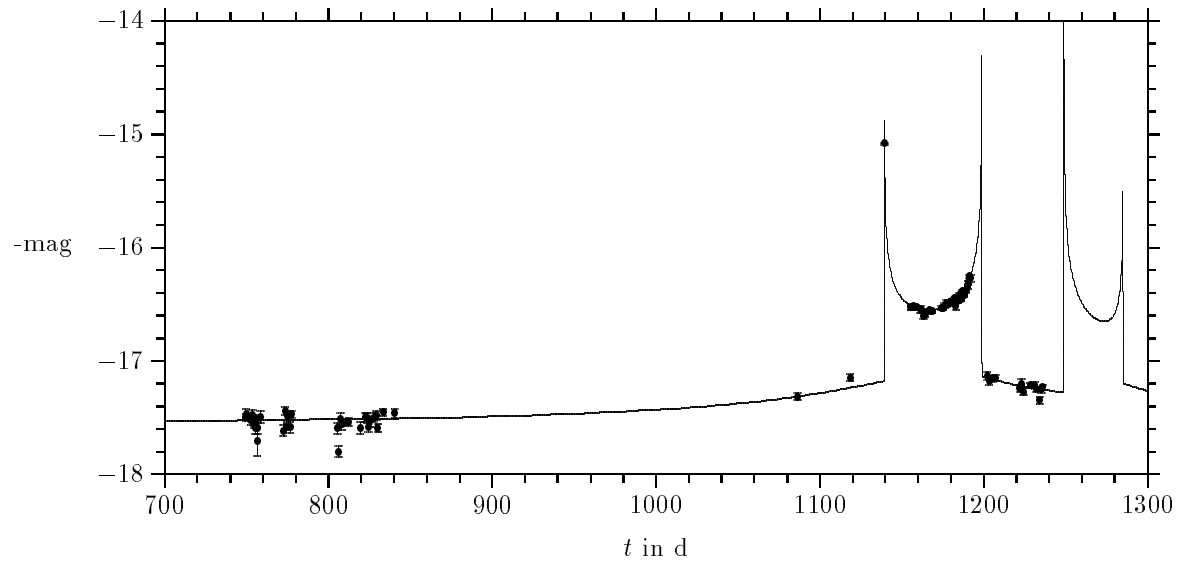


Figure 2f

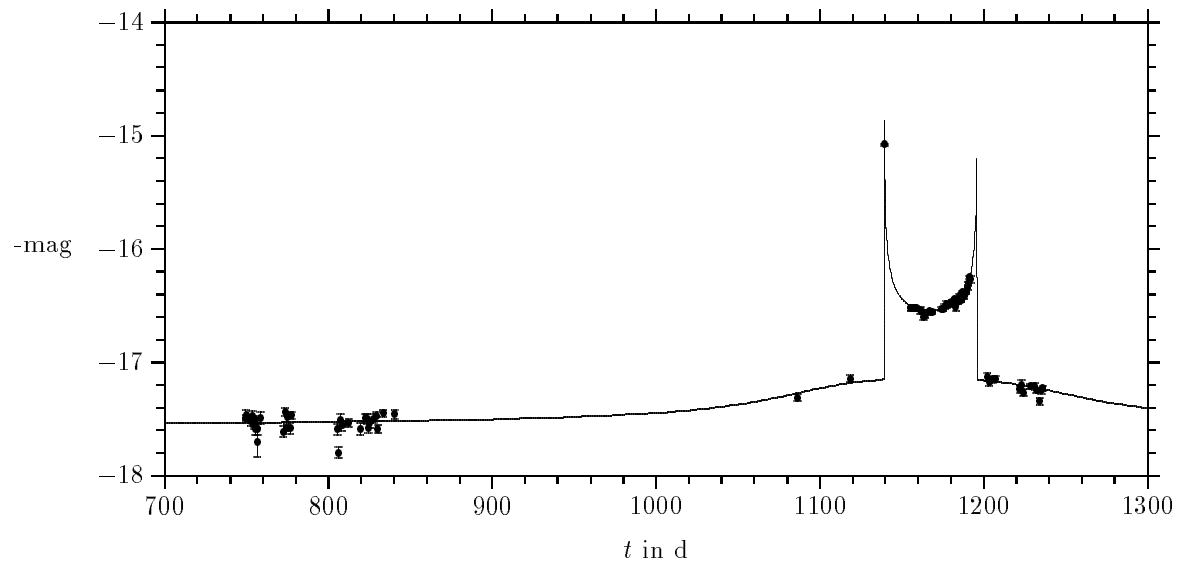


Figure 2g

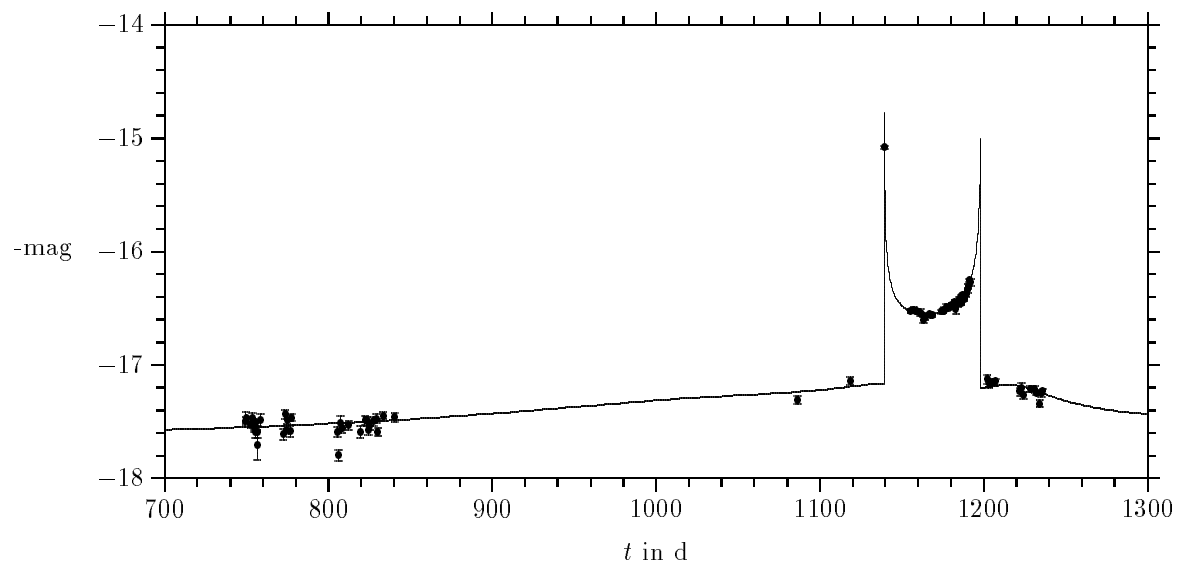


Figure 2h

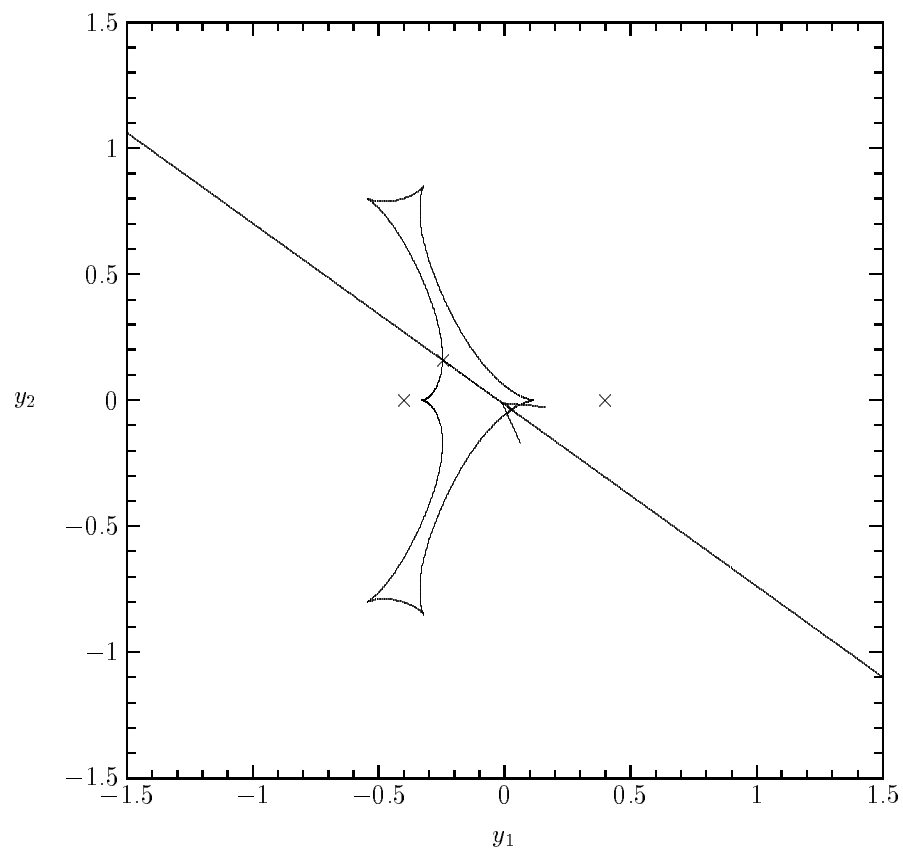


Figure 3a

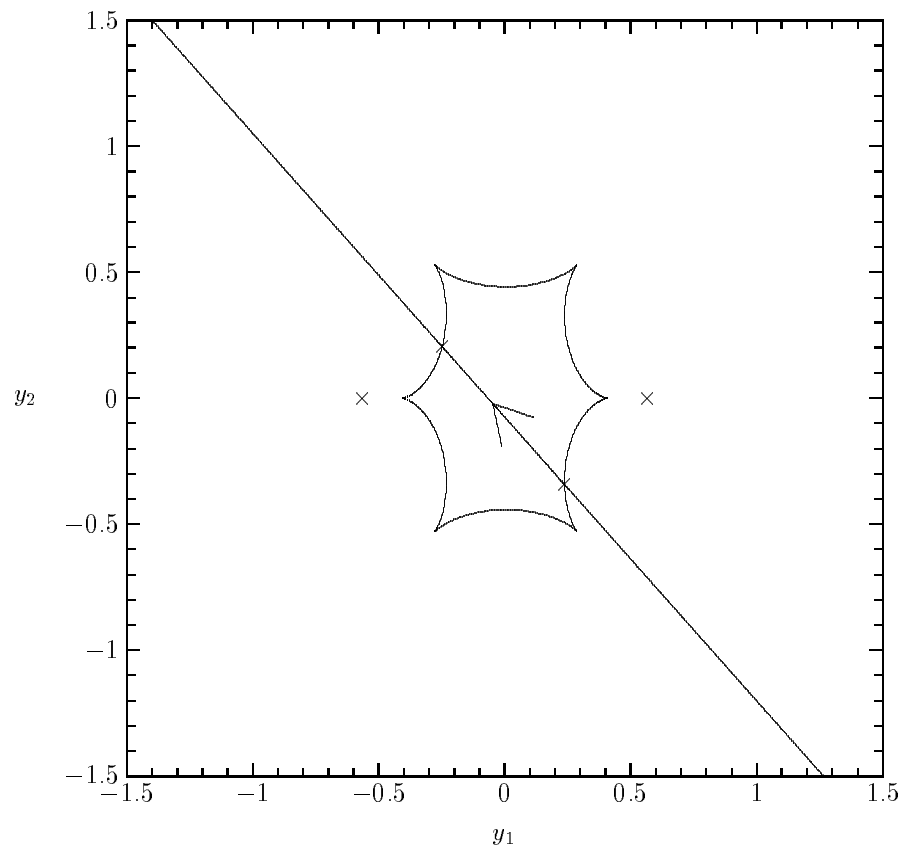


Figure 3b

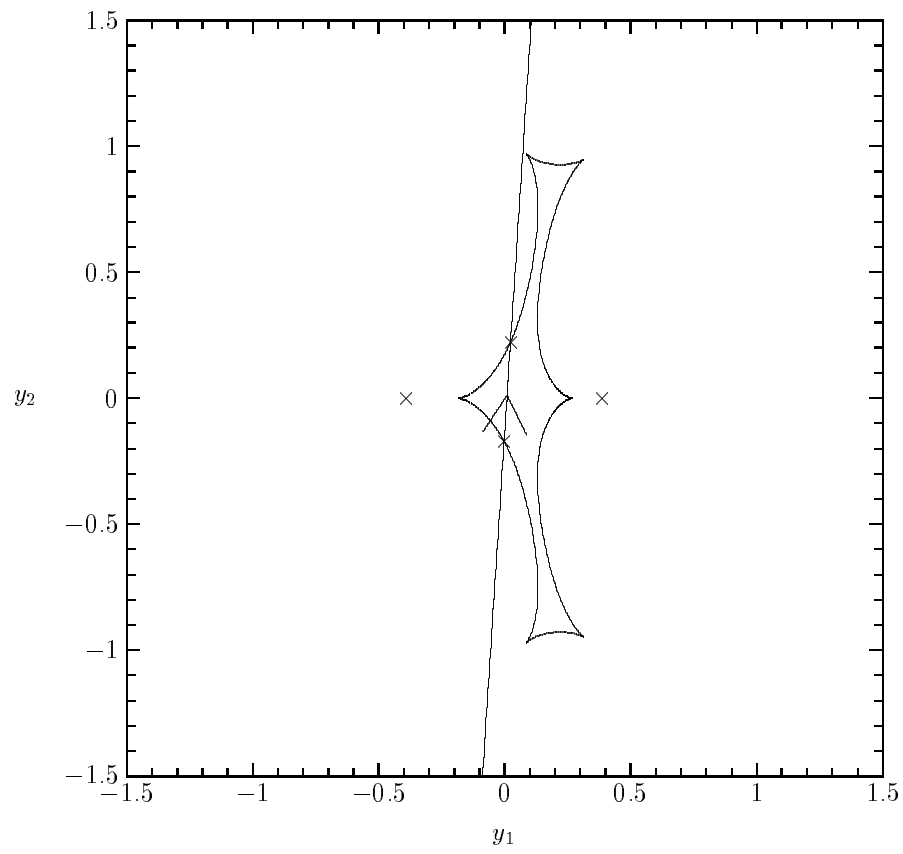


Figure 3c

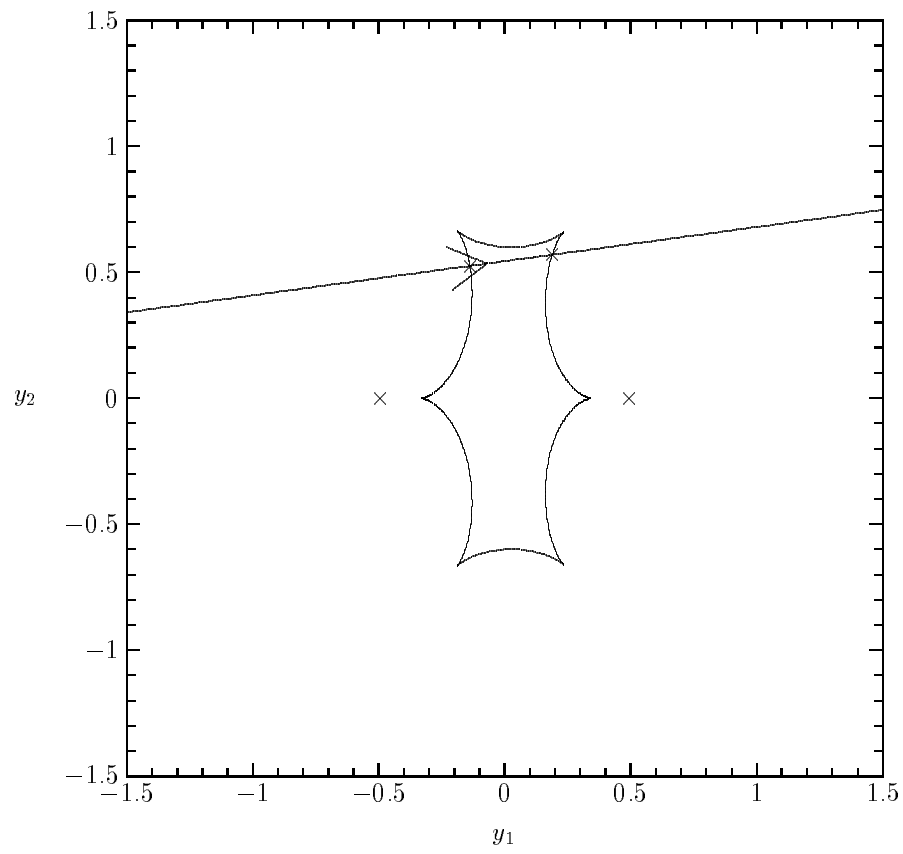


Figure 3d

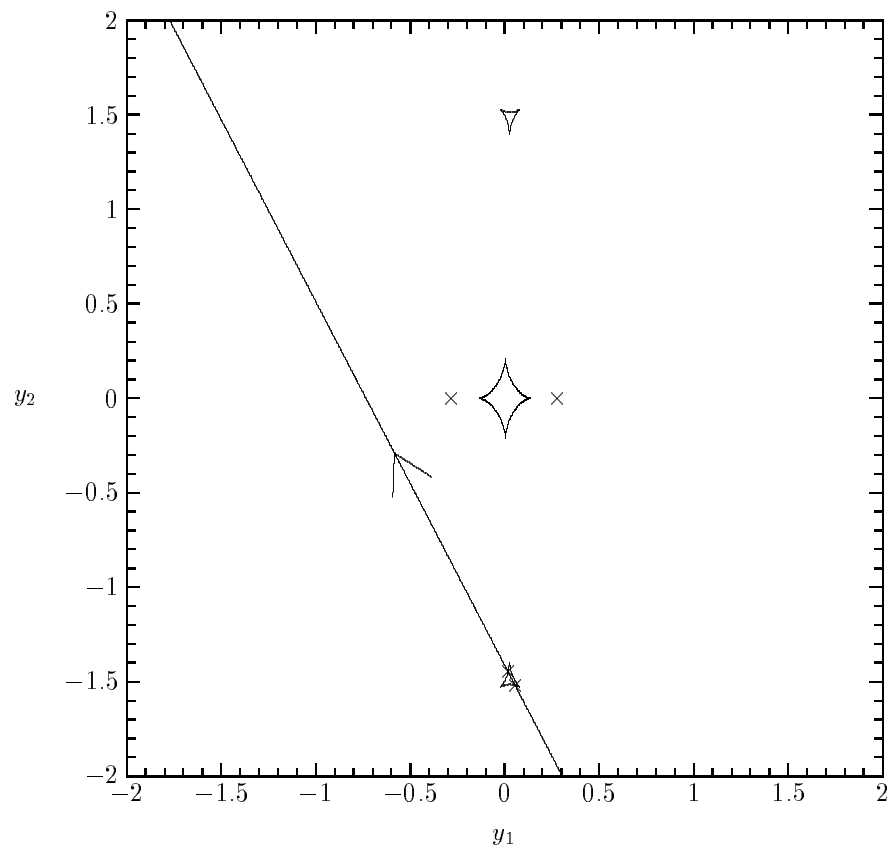


Figure 3e

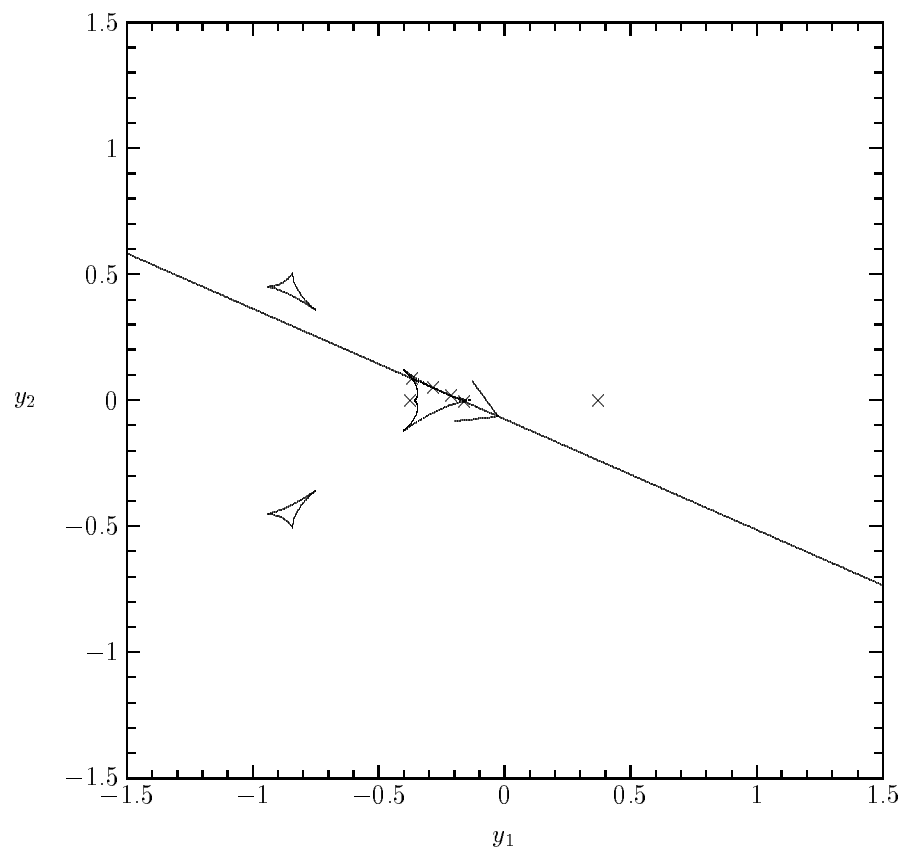


Figure 3f

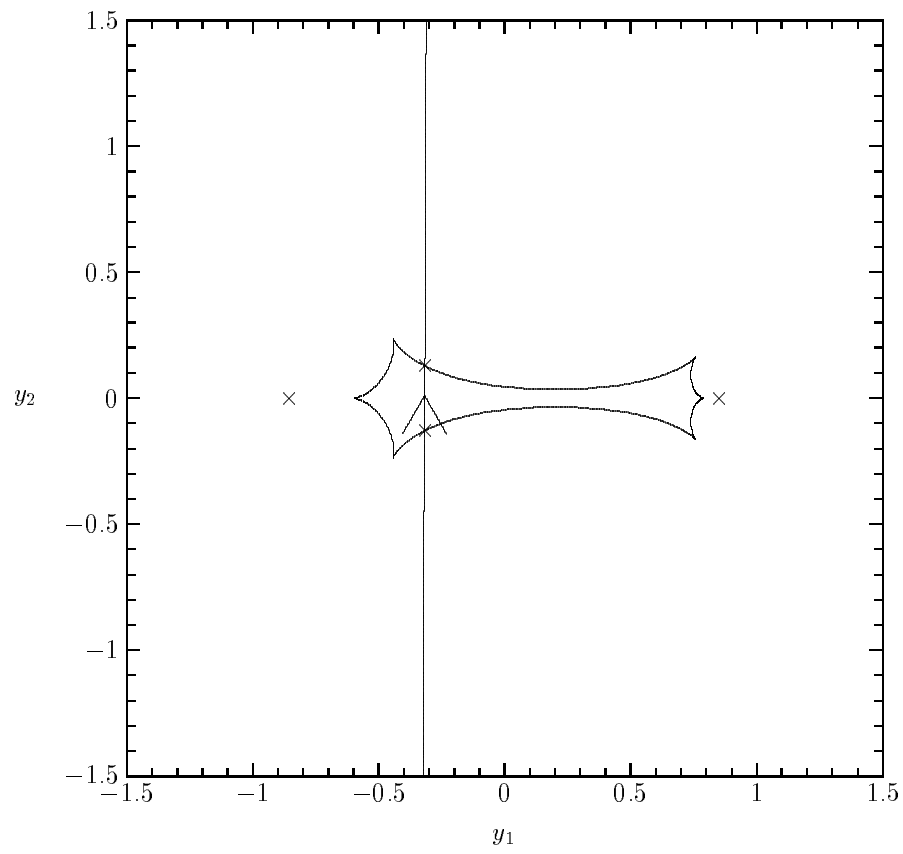


Figure 3g

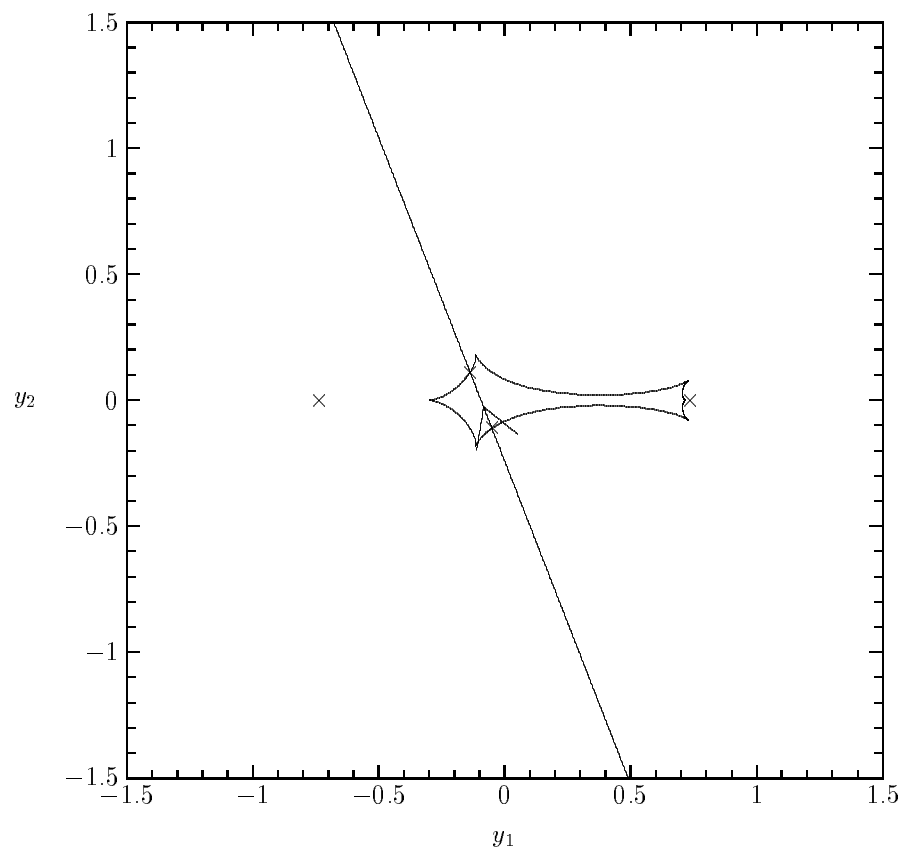


Figure 3h

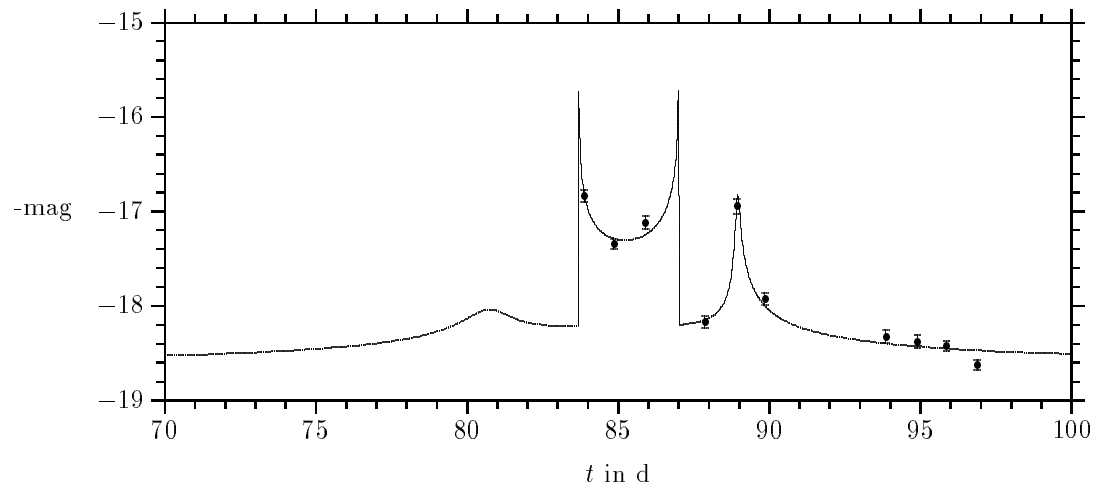
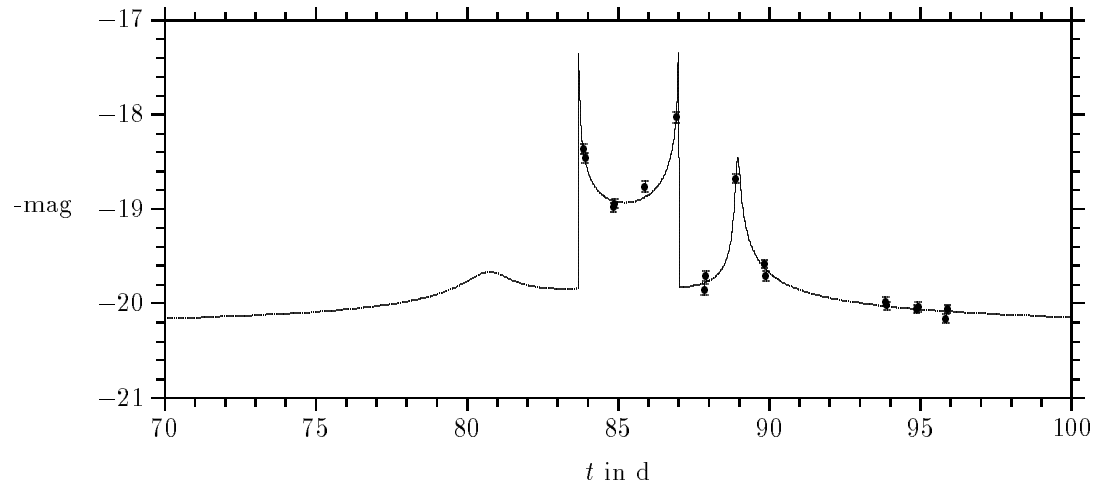


Figure 4a

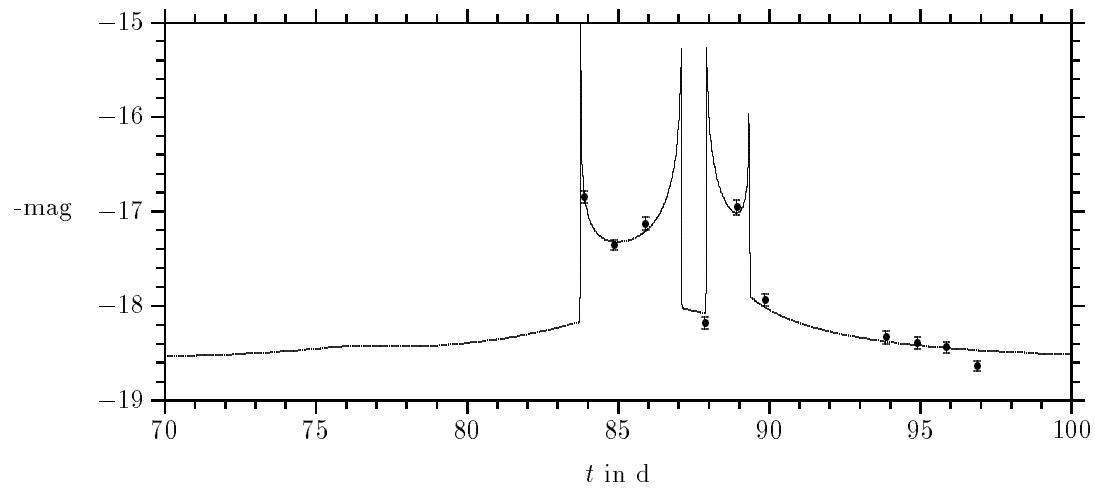
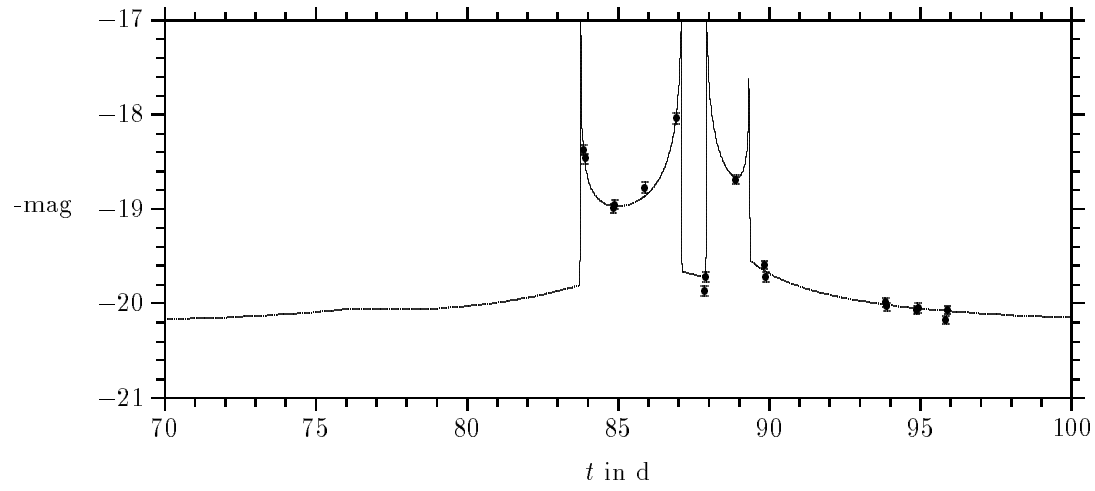


Figure 4b

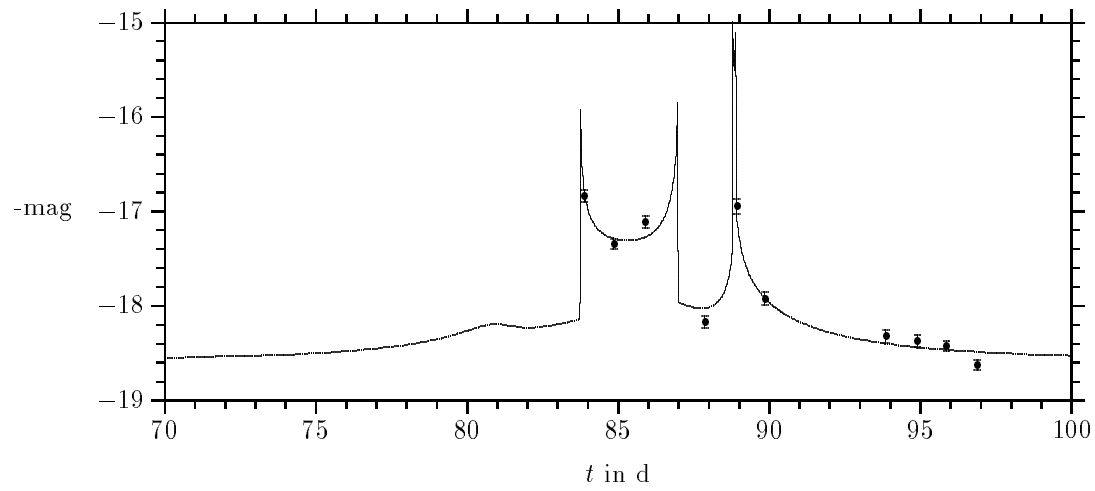
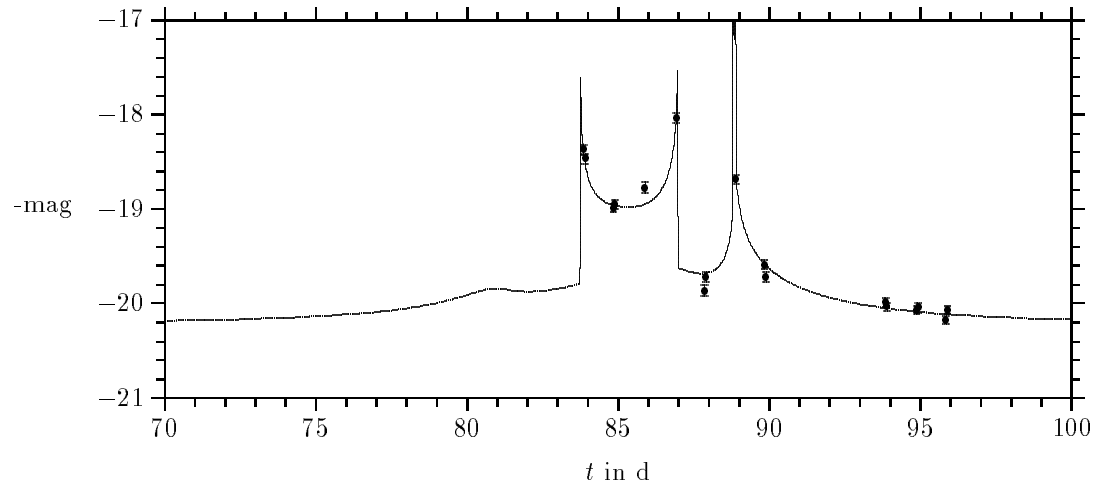


Figure 4c

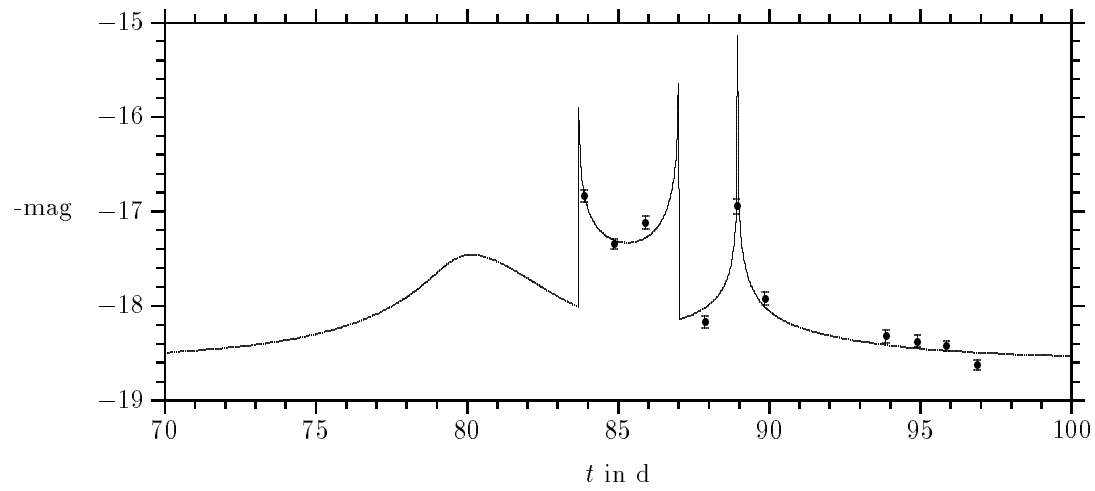
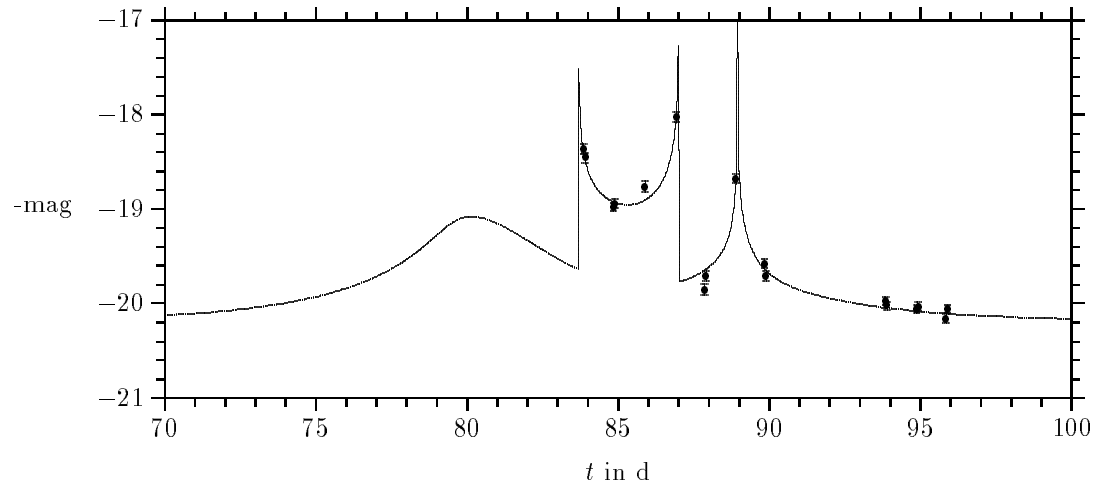


Figure 4d

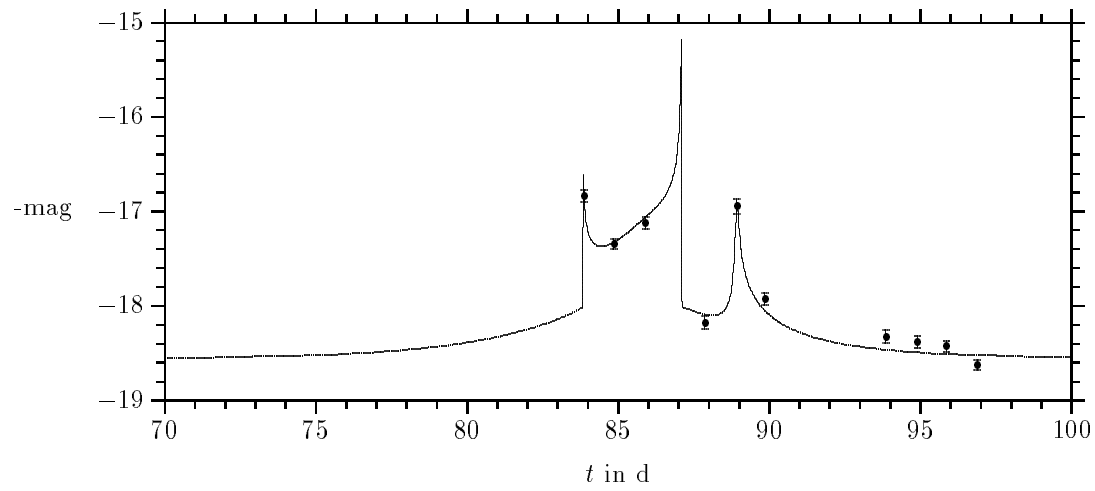
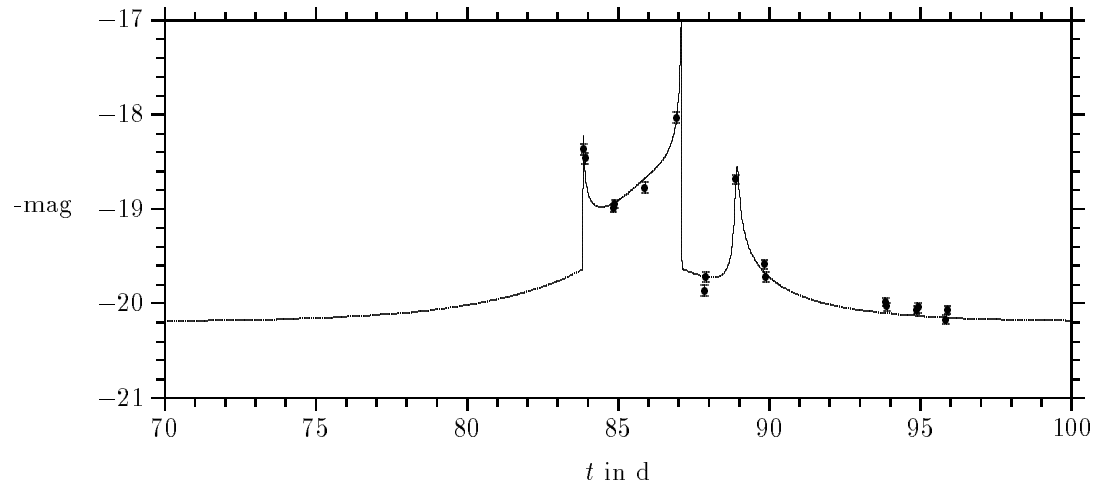


Figure 5a

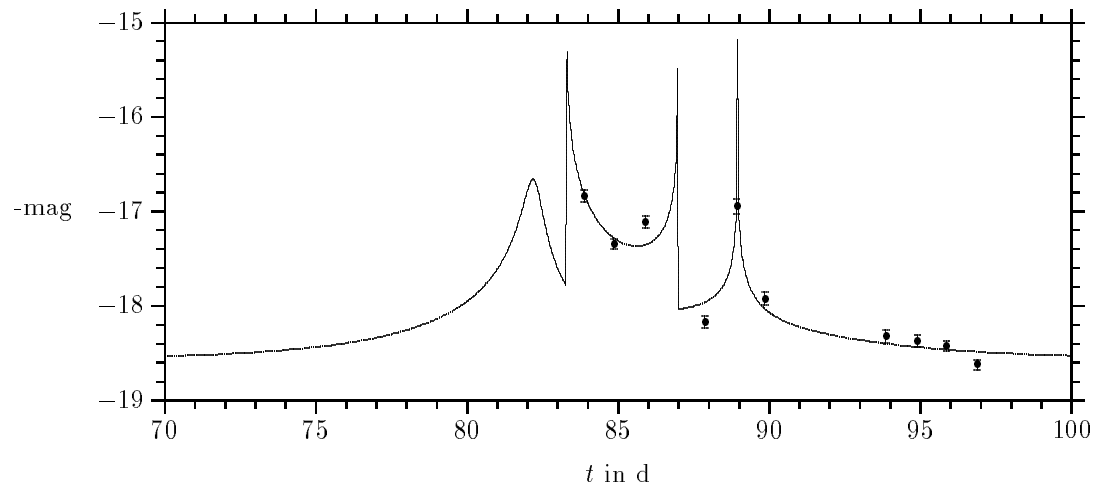
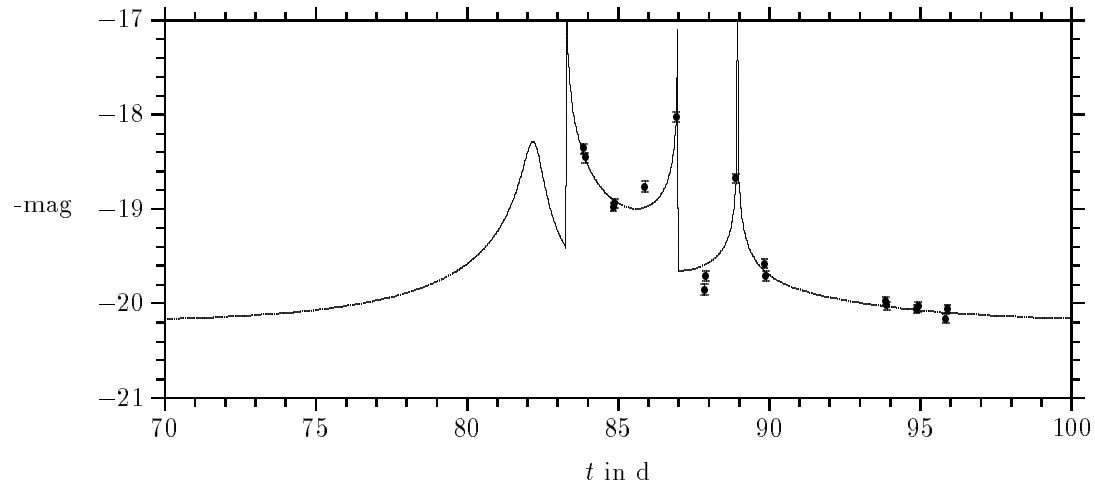


Figure 5b

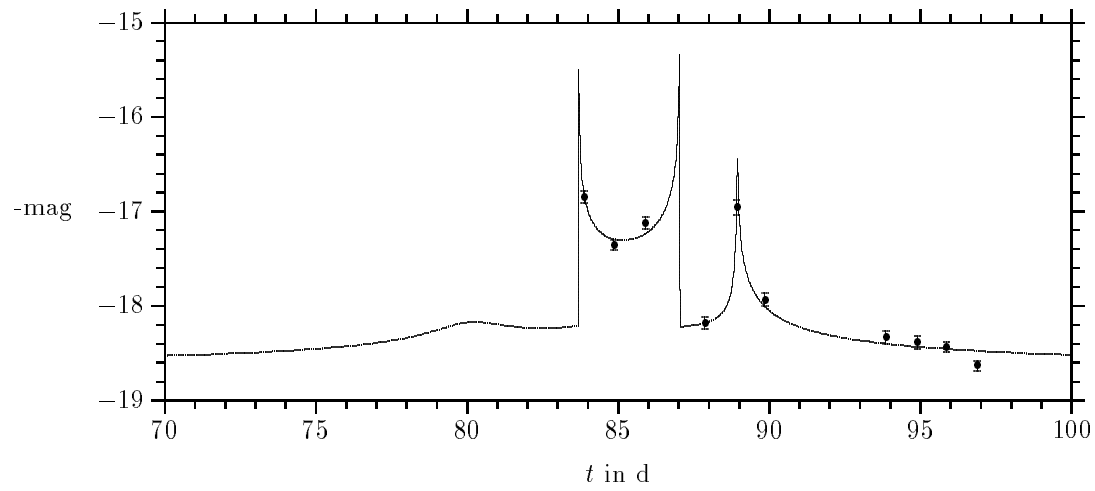
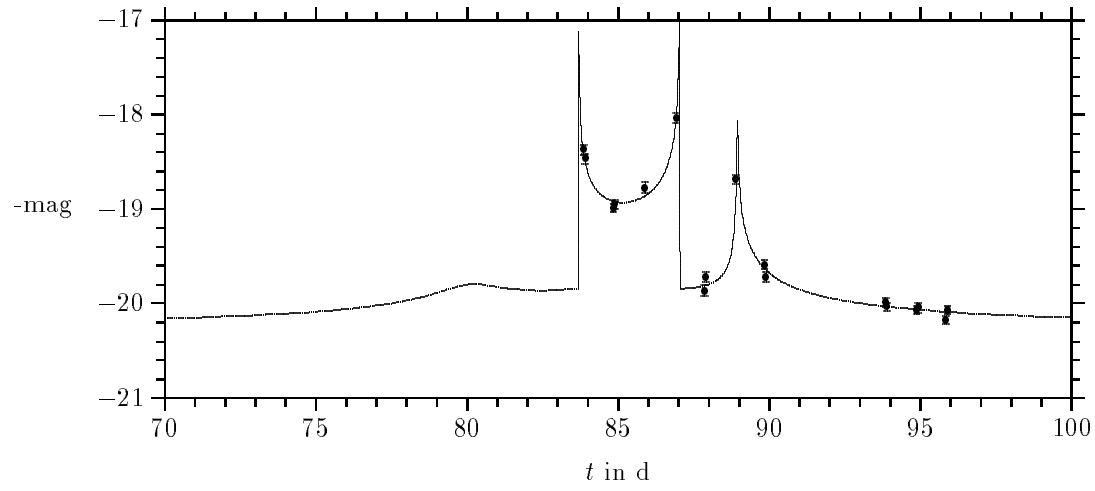


Figure 6

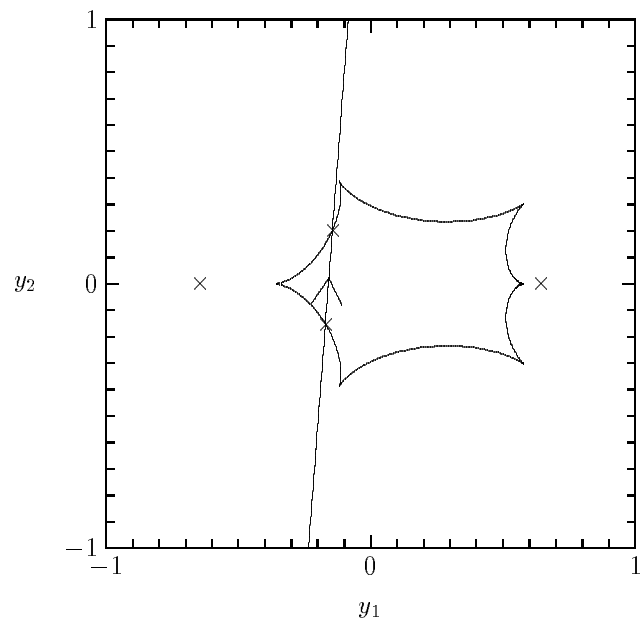


Figure 7a

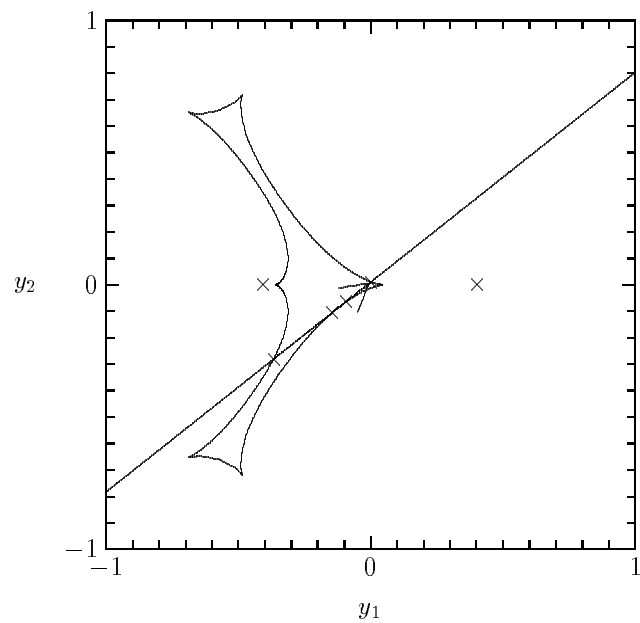


Figure 7b

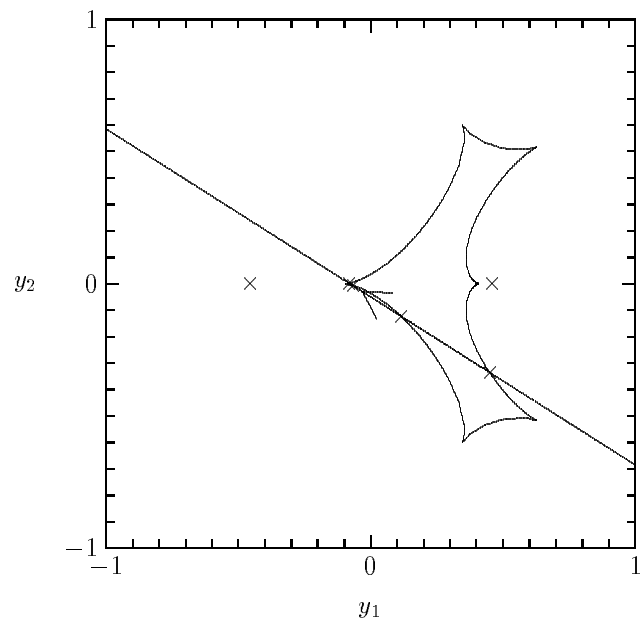


Figure 7c

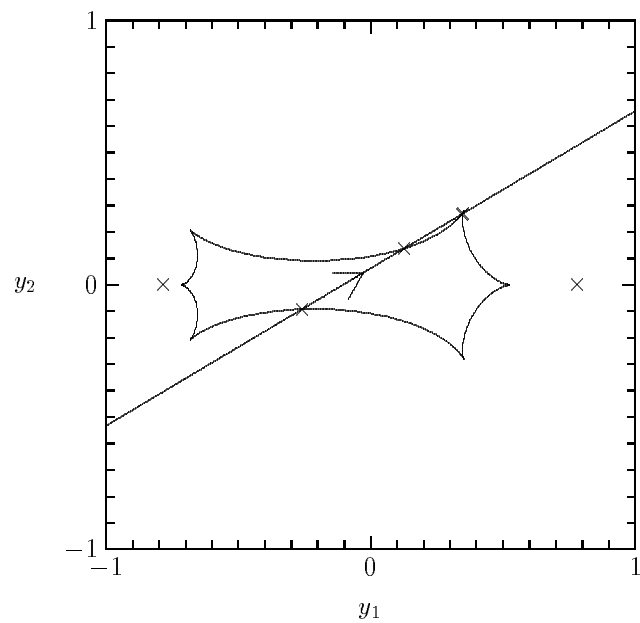


Figure 7d

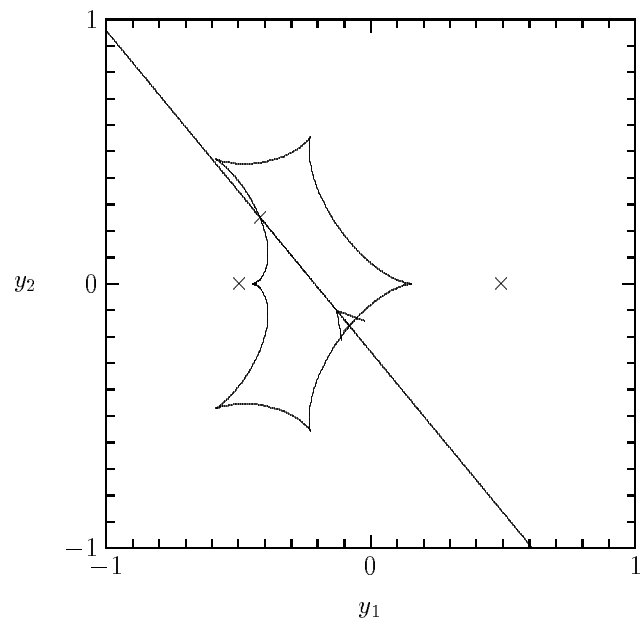


Figure 7e

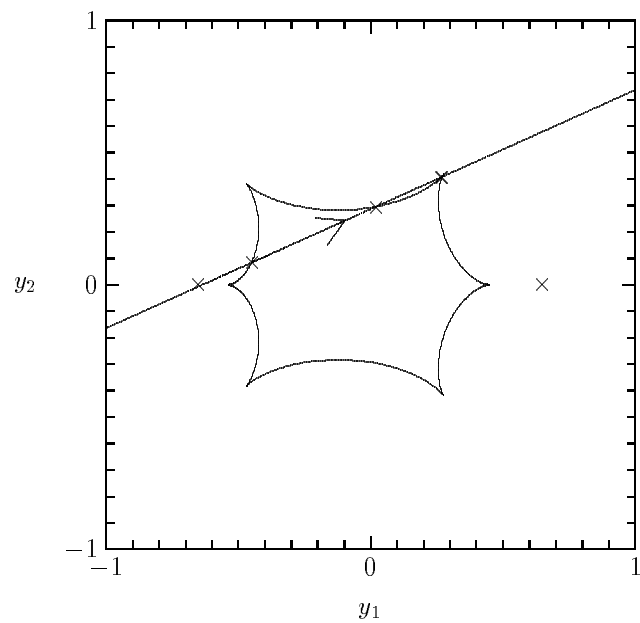


Figure 7f